PNAS
www.pnas.org

Supplementary Information for

Chemical depletion of phagocytic immune cells in *Anopheles gambiae* reveals dual roles of mosquito hemocytes in anti-*Plasmodium* immunity

Hyeogsun Kwon[1] and Ryan C. Smith[1*]

[1]Department of Entomology, Iowa State University, Ames, Iowa, 50011, USA

*Correspondence: smithr@iastate.edu

This PDF file includes:

www.pnas.org/cgi/doi/10.1073/pnas.1900147116

Supplemental Methods

RNA-Seq and differential gene expression analysis

Libraries were prepared by the Iowa State University DNA Facility using the TruSeq Stranded mRNA Sample Prep Kit (Illumina) using dual indexing according to the manufacturer's instructions. The size, quality, and concentration of the libraries was measured using an Agilent 2100 Bioanalyzer and a Qubit 4 Fluorometer (Invitrogen), then diluted to 2 nM based on the size and concentration of the stock libraries. Clustering of the libraries into a single lane of the flow cell was performed with an Illumina cBot. 150 base paired end sequencing was performed on an Illumina HiSeq 3000 using standard protocols.

Raw sequencing data was analyzed by the Iowa State genome Informatics Facility. Sequence quality was assessed using FastQC (v 0.11.5) (1), then paired end reads were mapped to the *Anopheles gambiae* PEST reference genome (AgamP4.9) downloaded from VectorBase (2) using STAR aligner (v 2.5.2b) (3). Genome indexing was performed using the genomeGenerate option and corresponding GTF file downloaded from VectorBase (version 4.7) followed by mapping using the alignReads option. Output SAM files were sorted and converted to BAM format using SAMTools (v 1.3.1) (4), and counts for each gene feature were determined from these alignment files using featureCounts (v 1.5.1) (5). Reads that were multi-mapped, chimeric, or fragments with missing ends were excluded. Counts for each sample were merged using AWK script and differential gene expression analyses was performed using edgeR (6). Differentially expressed genes with a q-score ≤ 0.1 were considered significant and were used for downstream analyses. Gene expression data have been deposited in NCBI's Gene Expression Omnibus (7) and are accessible through GEO Series accession number GSE116156 (https://www.ncbi.nlm.nih.gov/geo/query/acc.cgi?acc=GSE116156).

Several candidate genes identified in our RNA-seq expression analysis were selected and measured by qRT-PCR to further validate the results of our gene expression experiments. Transcripts influenced by phagocyte depletion were selected according to significant fold-change values. Independent mosquito carcass samples ~24 h post-*P.*

berghei infection were prepared from pre-treated liposome mosquitoes samples and were used for validation experiments. Total RNA isolation, cDNA synthesis and qRT-PCR were performed as described above. These same samples were used for additional follow-up experiments examining PPO gene expression. In addition, relative PPO gene expression was determined in total hemocyte samples collected from perfused hemolymph (n=60) following LP and CLD treatment in infected (~24 h) *P. berghei* mosquitoes. RNA was isolated using TRIzol and was then further purified with RNA Clean & Concentrator-5 kit. Total RNA (200 ng) was used for cDNA synthesis. Primers used are listed in *SI Appendix*, Table S3.

Gene silencing by dsRNA

RNAi experiments were performed with selected genes: *PPO2* (AGAP006258), *PPO3* (AGAP004975), *PPO4* (AGAP004981), *PPO5* (AGAP012616), *PPO6* (AGAP004977), *PPO9* (AGAP004978), *CLIPD1* (AGAP002422) and a putative leucine-rich immunomodulatory (LRIM) protein (AGAP001470). T7 primers were designed using the E-RNAi web application (http://www.dkfz.de/signaling/e-rnai3/idseq.php) and listed in Table S3. T7 templates for dsRNA synthesis were amplified from cDNA prepared from whole mosquitoes ~24 h post-*P. berghei* infection. PCR amplicons were purified using the DNA Clean & Concentration kit (Zymo Research). dsRNAs were synthesized using the MEGAscript RNAi kit (Life Technologies) according to the manufacturer's instructions, and then resuspended in nuclease free water to 3 µg/µl after ethanol precipitation. Three to four day old mosquitoes were cold anesthetized and injected in the thorax with 69 nl (~200 ng) of dsRNA per mosquito. The effects of gene silencing were measured 2 days post-injection in whole mosquitoes (n=15) by qRT-PCR as described above. Although dsRNA targeting each individual PPO target gene were prepared following E-RNAi design (8), potential off-target effects on other PPO gene family members were examined to determine if the knockdown of a specific PPO dsRNA influences the expression of other PPO transcripts. Primers used to evaluate gene silencing by qRT-PCR experiments are listed in Table S2. To evaluate the effects of gene-silencing on malaria parasite infection, mosquitoes were challenged with *P. berghei* 2 days post-injection of dsRNA. Oocyst numbers were examined at either 2 days or 8 days post-infection.

Western blot analysis

Following liposome treatments, hemolymph was perfused from individual mosquitoes (n=15) at naïve or 24 h *P. berghei*-infected mosquitoes using incomplete buffer (anticoagulant solution without fetal bovine serum) containing a protease inhibitor cocktail (Sigma) (9). Hemolymph protein concentrations were measured using Quick Start™Bradford Dye reagent (Bio-Rad). Protein samples (~2 µg) were mixed with Bolt™LDS sampling buffer and sample reducing agent (Life Technologies), and heated at 70°C for 5 min before separated on 4-12% Bis-Tris Plus ready gel (Thermo Fisher Scientific). Samples were resolved using Bolt™MES SDS running buffer (Thermo Fisher Scientific) for 90 min at 100 V. Proteins were transferred to PVDF membrane in Bolt™Transfer buffer (Life Technologies) for 1 h at 20 V, and then blocked in TBST buffer (10 mM Tris base, 140 mM NaCl, 0.05% Tween 20, pH 7.6) containing 5% non-fat milk for 1 hour at RT. For western blotting, the membrane was incubated with a 1:1000 dilution of rabbit anti-TEP1 (10), rabbit anti-PPO6 , or rabbit anti-serpin3 (SRPN3) antibodies (11) in TBST blocking buffer overnight at 4°C. Membranes were washed three times for 5 min in TBST, then incubated with a secondary anti-rabbit alkaline phosphatase-conjugated antibody (1:7500, Thermo Fisher Scientific) for 2 h at RT. Following washing in TBST, the membrane was incubated with 1-Step™NBT/BCIP (Thermo Fisher Scientific) to enable colorimetric detection. For comparative analysis between samples, densitometric analysis of protein bands was performed using ImageJ (https://imagej.nih.gov/ij/).

Supplemental Figures

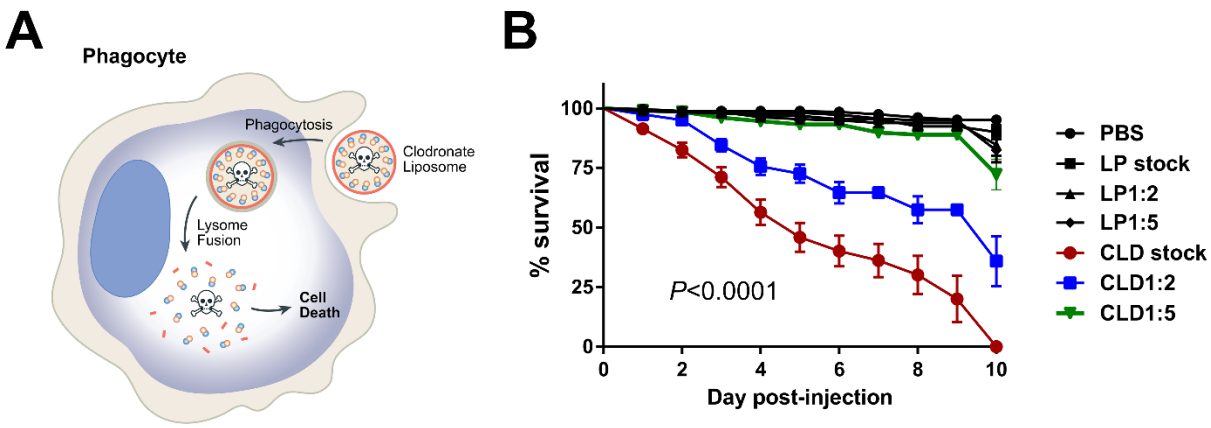

Fig. S1. Overview of clodronate liposome function and its optimization in *An. gambiae.* Based on work form other systems, the current model of clodronate liposome function suggests that following phagocytosis, liposomes are degraded by lysosomal fusion to release clodronate intracellularly inhibiting ATP/ADP transport resulting in cell death (**A**). To determine the ideal concentration of clodronate liposomes (CLD), mosquito survival was evaluated following the injection of control liposomes (LP) or CLD at stock or diluted concentrations (1:2, 1:5) in addition to 1x PBS (**B**). Survival was measured each day for a total of ten days. Error bars represent mean ± SEM of three independent replicates. In each replicate, 30 female mosquitoes were used for each experimental treatment. Significance was determined by a Log-rank (Mantel-Cox) test using GraphPad Prism 6.0.

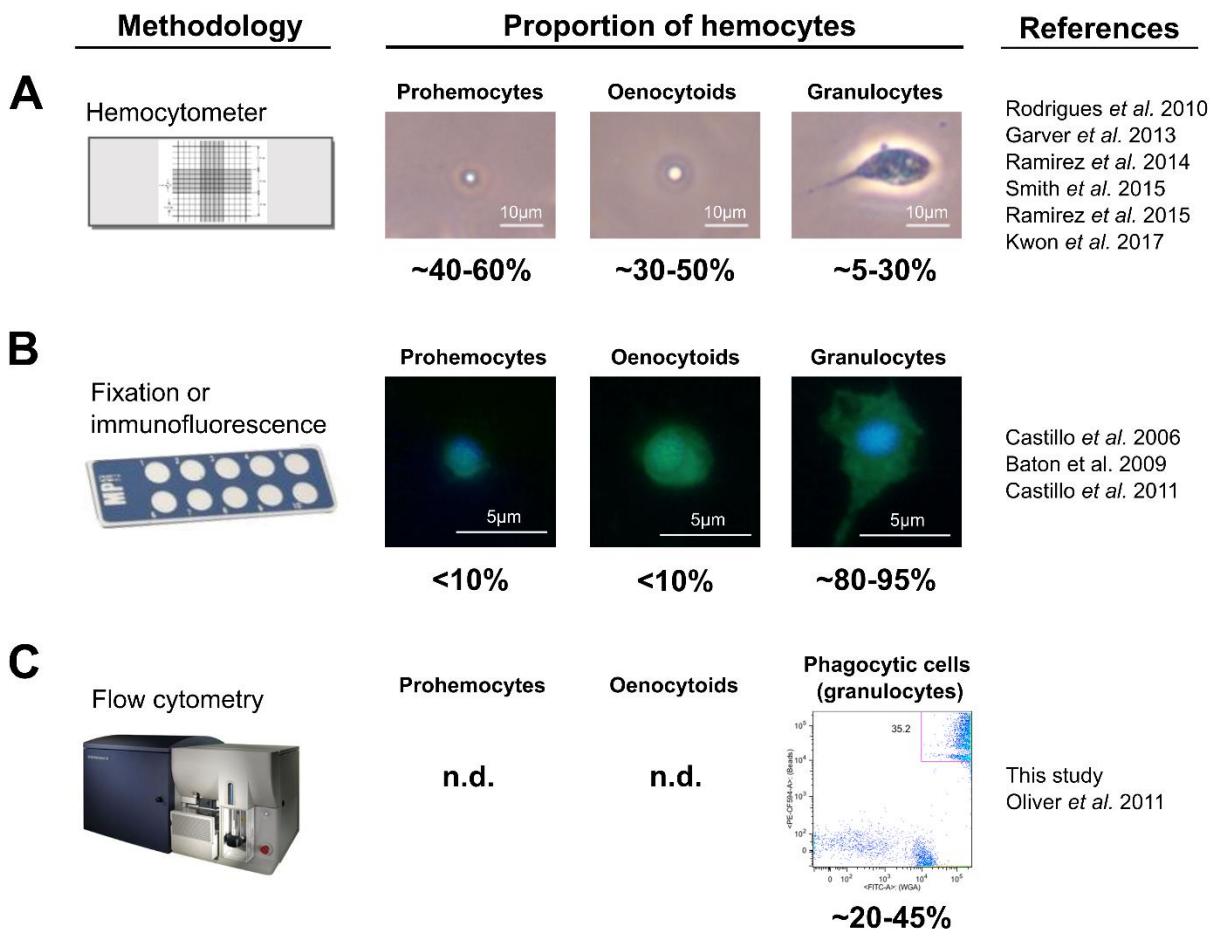

Fig. S2. Methods for the analysis of mosquito hemocyte populations. Multiple methodologies have been used to examine mosquito hemocytes with different experimental outcomes in the percentages of each hemocyte sub-type. Without genetic markers or antibodies, these assays are largely based on size and morphological characteristics, the propensity to adhere and spread on a slide, and phagocytic activity. After perfusion, samples can be immediately analyzed using a hemocytometer (**A**), allowed to adhere and then be fixed onto a glass slide for microscopy or immunofluorescence (**B**), or can be stained in solution for flow cytometry analysis (**C**). This results in a wide range of percentages for each of the three hemocyte sub-types (prohemocyte, oenocytoid, and granulocyte) from these methodologies. Examples of each cell type are shown under each of the respective methods (**A-C**), with the range of hemocyte percentages displayed for that respective cell type. References for each of these techniques and their resulting outcomes are shown on the right. At present, there are no methods currently available to select for prohemocyte and oenocytoid populations (n.d.) using flow cytometry analysis (**C**). References for each method are shown on the right (12–21). Percentages of each cell type are taken from a range of naïve, blood-fed, and *Plasmodium*-infected mosquitoes. Images in (**A**) and (**B**) are taken from naïve adult female mosquitoes, while data in (**C**) is from *P. berghei* infected mosquitoes 24h post-infection.

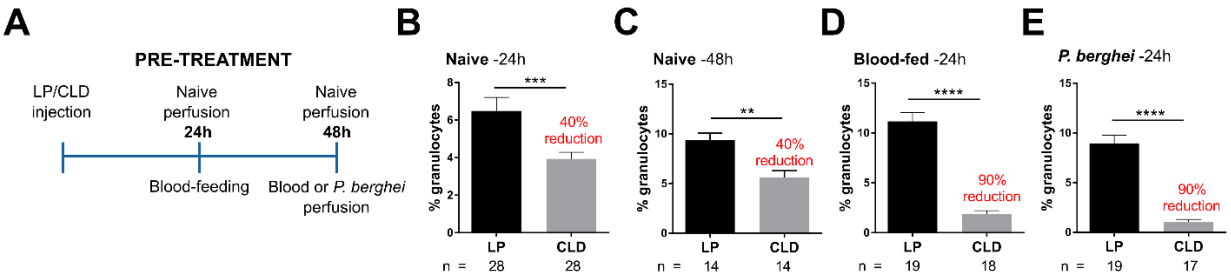

Fig. S3. Validation of phagocyte depletion using light microscopy after clodronate liposome (CLD) treatment. Experimental overview of hemolymph perfusion from pre-treated mosquitoes at naïve, blood feeding or *P. berghei* infection to evaluate the effects of clodronate liposomes in *An. gambiae* (**A**). Following hemolymph perfusion, the depletion of phagocytic granulocytes was examined by morphology from control liposomes (LP) and CLD-treated mosquitoes under naïve conditions at 24 (**B)** and 48 hrs (**B**), as well as at 24 hr post-challenge with a non-infectious blood meal (**D**) or *P. berghei* infection (**E**). Data were analyzed using a Mann–Whitney test on GraphPad Prism 6.0. Data represent the mean ± SEM of three independent experiments. n= the number of mosquitoes examined for each condition. Asterisks denote significance (***P* < 0.01, ****P* < 0.001, *****P* < 0.0001).

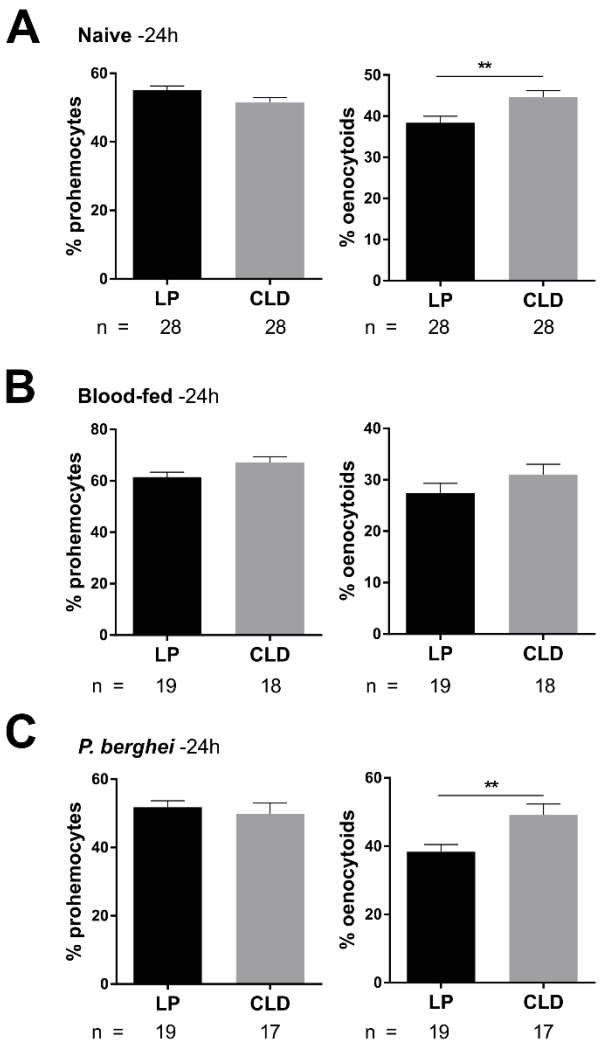

Fig. S4. Clodronate liposome (CLD) treatment does not reduce the relative proportion of non-target hemocyte subtypes. Following hemolymph perfusion, the proportion of non-phagocytic hemocyte subtypes (prohemocyte and oenocytoid) were evaluated on a hemocytometer and examined by morphology from control liposomes (LP) and CLD-treated mosquitoes under naïve conditions at 24 hrs (**A)**, and 24 hrs post-feeding with a non-infectious blood meal (**B**) or *P. berghei*-infected blood (**C**). Data were analyzed using a Mann–Whitney test with GraphPad Prism 6.0. Data represent the mean ± SEM of three independent experiments. n= the number of mosquitoes examined for each condition. Asterisks denote significance (**$P < 0.01$, ***$P < 0.001$, ****$P < 0.0001$). Data were collected from the same samples presented in Fig. S3.

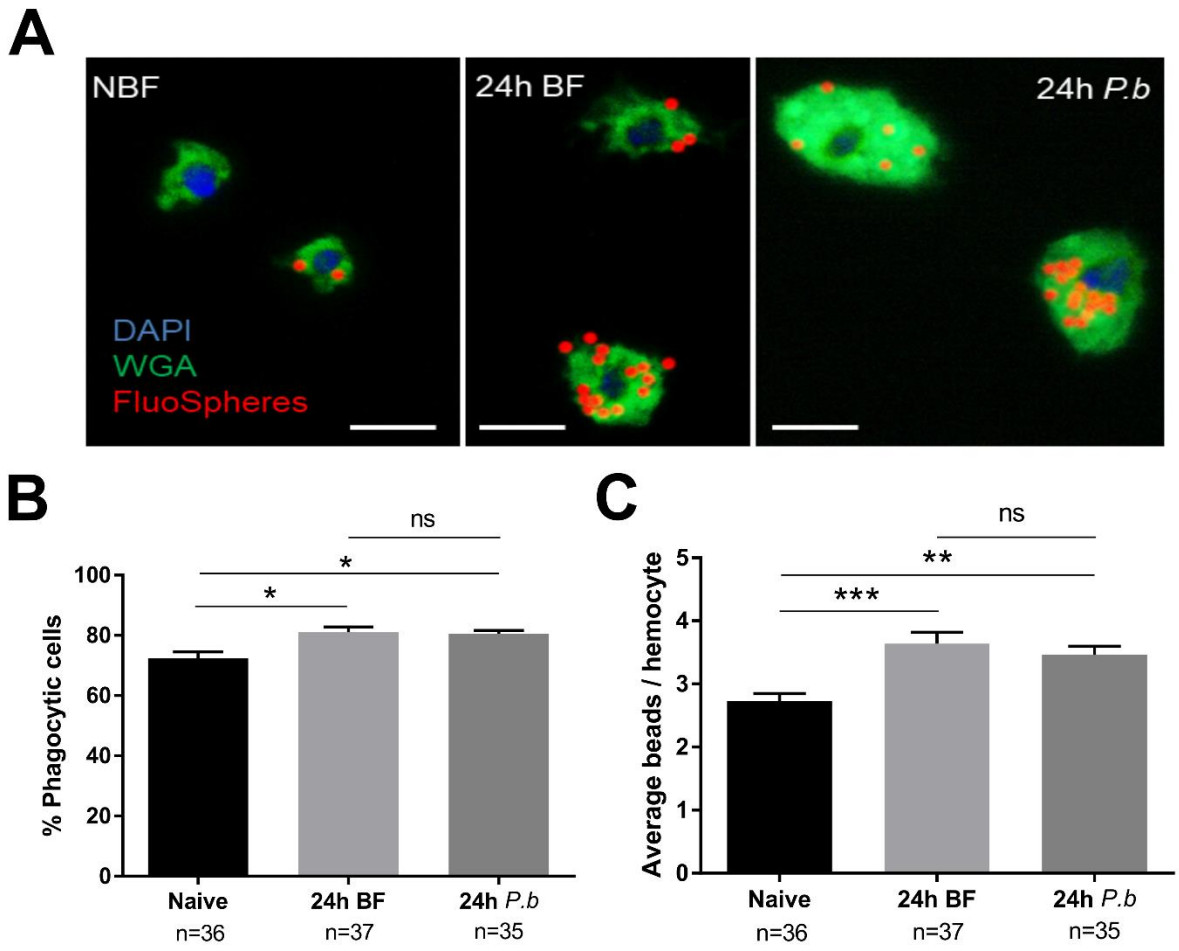

Fig. S5. Phagocytic activity increases following blood-feeding, independent of infection status. Phagocytosis assays were performed under naïve, blood-fed (BF), or *P. berghei (P.b.)*-infected conditions, with representative images from each experimental condition displayed in (**A**). Cells from each experimental condition were evaluated as the % of phagocytic cells (**B**) and the phagocytic index (number of beads per cell) (**C**). Three independent experiments were performed. Data were analyzed by Kruskal-Wallis with a Dunn's post-test using GraphPad Prism 6.0. n= the number of mosquitoes examined for each condition. Asterisks denote significance (*$P < 0.05$, **$P < 0.01$, ***$P < 0.001$); ns, not significant. Scale bar: 10 µm.

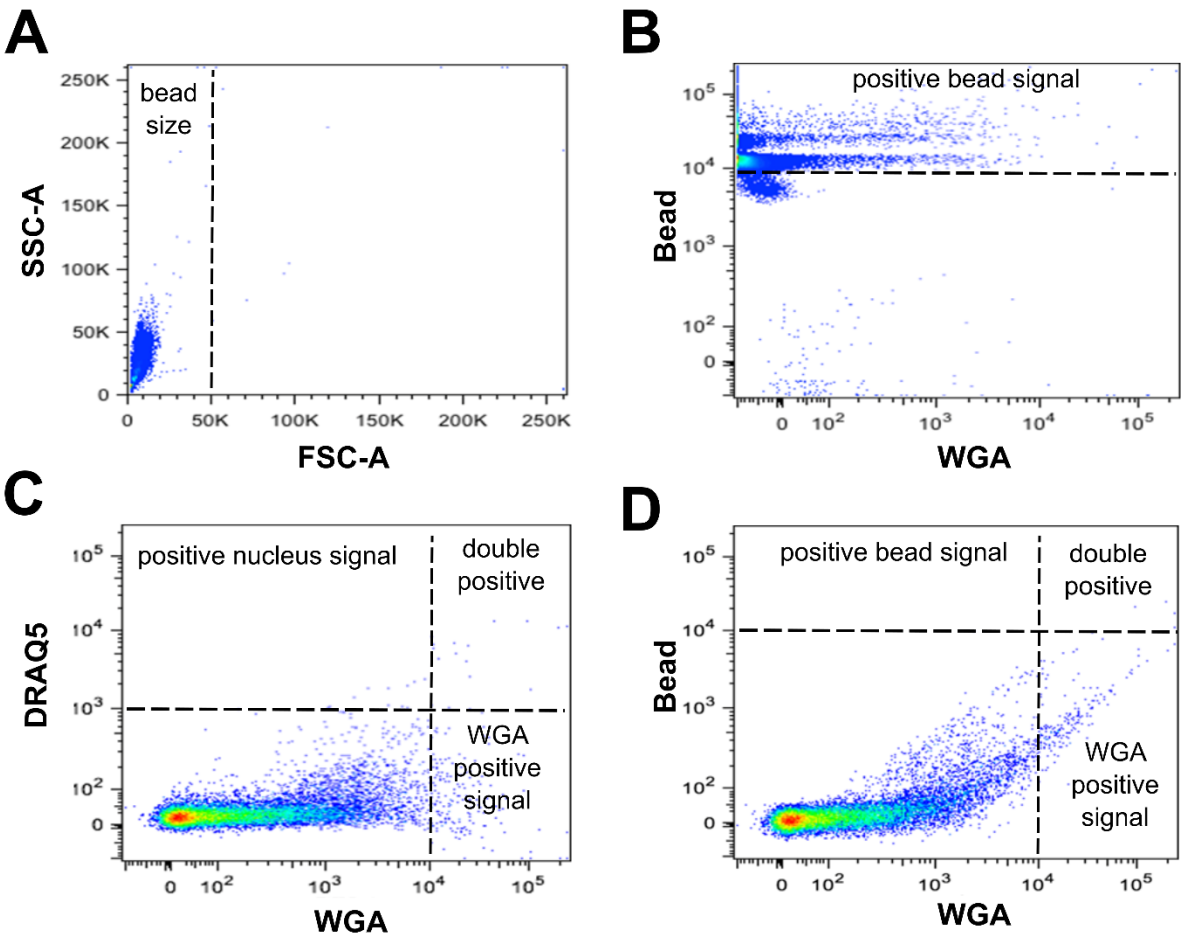

Fig. S6. Determination of threshold values for flow-cytometry analysis. Before flow cytometry analyses, threshold values were determined using either red fluorescent beads (**A** and **B**) or with unstained hemocytes (**C** and **D**) to determine positive fluorescent signals in hemocytes following bead injection or WGA/DRAQ5 staining. This enabled size cutoffs by FSC (**A**) and the determination of signal cutoffs by fluorescent bead signal (**B**). Basal levels of auto-fluorescence were determined to identify WGA^+/DRAQ5+ cells (**C**) as well as WGA^+/$bead^+$ cells indicative of phagocytic capacity (**D**).

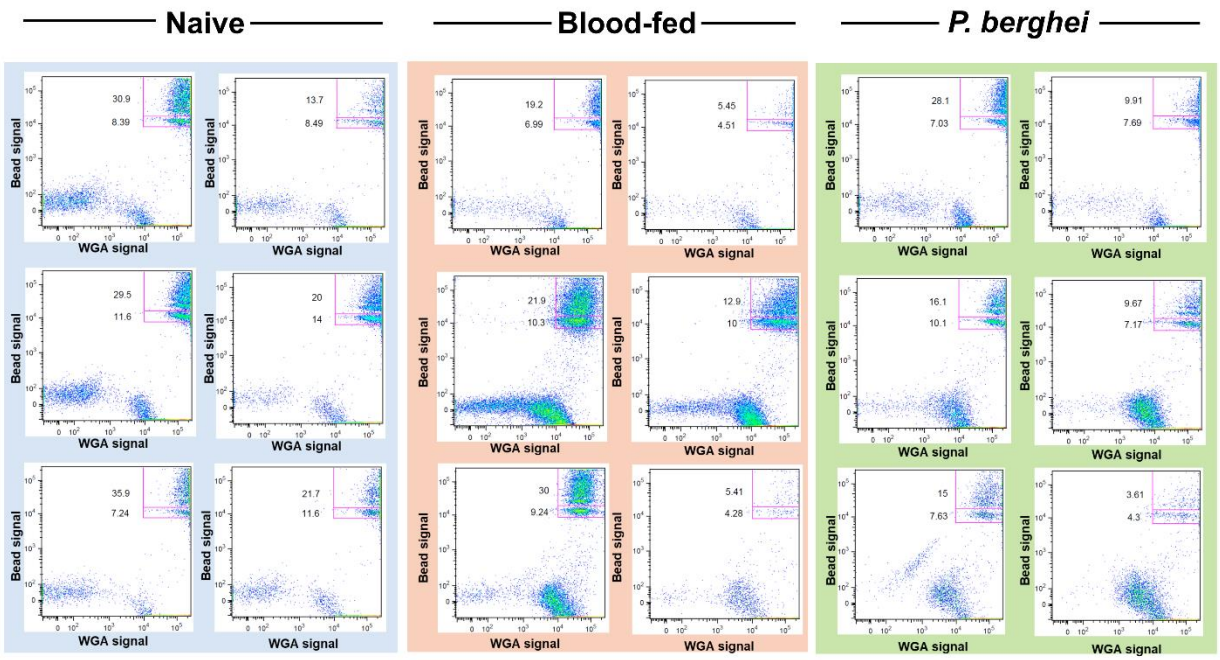

Fig. S7. Flow-cytometry analyses of phagocyte depletion following control liposome (LP) and clodronate liposome (CLD) treatments. The proportion of phagocytic immune cells was measured from mosquito samples from three independent experiments under naive, 24 h blood fed, and 24 h *P. berghei*-infected physiological conditions.

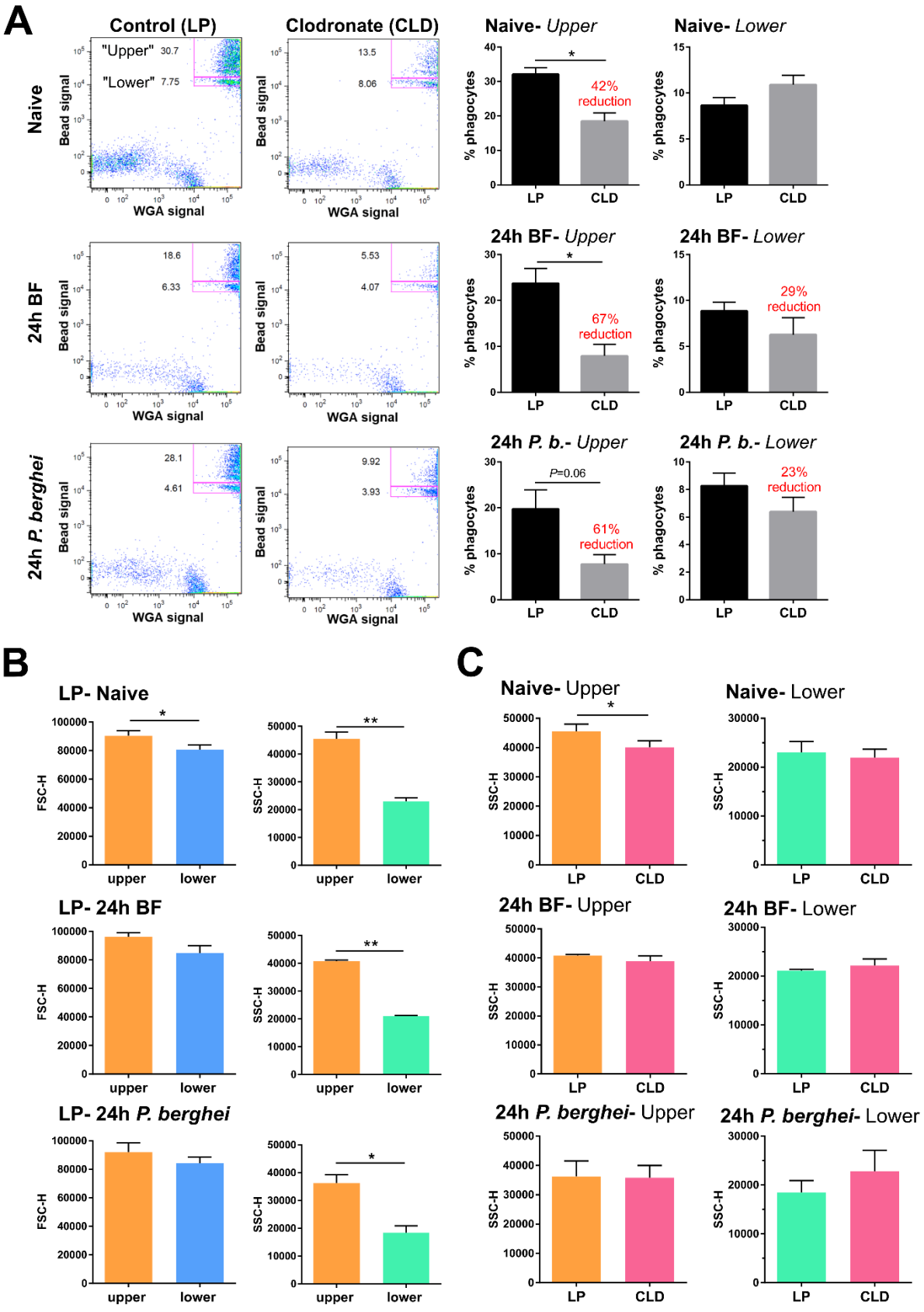
A
Control (LP)
Clodronate (CLD)
Naive
24h BF
24h P. berghei
"Upper" 30.7
"Lower" 7.75
13.5
8.06
18.6
6.33
5.53
4.07
28.1
4.61
9.92
3.93
Bead signal
WGA signal
Naive- Upper
Naive- Lower
24h BF- Upper
24h BF- Lower
24h P. b.- Upper
24h P. b.- Lower
% phagocytes
42% reduction
67% reduction
61% reduction
29% reduction
23% reduction
P=0.06
LP
CLD
B
LP- Naive
LP- 24h BF
LP- 24h P. berghei
FSC-H
SSC-H
upper
lower
C
Naive- Upper
Naive- Lower
24h BF- Upper
24h BF- Lower
24h P. berghei- Upper
24h P. berghei- Lower

Fig. S8. The efficacy of phagocyte depletion following clodronate treatment varies between sub-populations of phagocytic cells. Two distinct phagocyte populations were identified by flow cytometry analysis that were distinguished by the signal of phagocytosed fluorescent beads (**A**). These two populations were grouped into “upper” and “lower” populations, then examined across naive, 24 h blood fed, and 24 h *P. berghei*-infected physiological conditions to examine differences in responses to clodronate treatment (CLD) when compared to control liposomes (LP) (**A**). Phagocytes in the upper populations were more susceptible to be depleted by clodronate liposomes than those in the lower populations (**A**). Phagocytic “upper” and “lower” populations were evaluated by cell size (FSC) and granularity (SSC) in LP control mosquitoes under different physiological conditions (**B**). Comparisons of upper and lower phagocyte populations were also evaluated by granularity (SSC) between LP and CLD treatments under different physiological conditions (**C**). Bar graphs represent the mean ± SEM. Data were analyzed by unpaired *t*-test using GraphPad Prism 6.0. Asterisks denote significance (*$P < 0.05$, **$P < 0.01$).

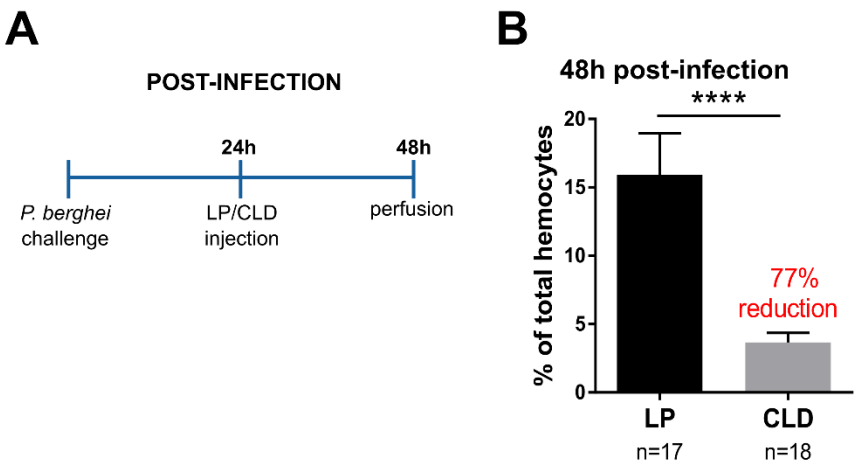

Fig. S9. Post-infection treatment of clodronate liposomes after *P. berghei* infection. Experimental overview of control liposome (LP) and clodronate (CLD) treatments after mosquitoes were infected with *P. berghei* (**A**). One day later, hemolymph was perfused from LP- and CLD-treated mosquitoes and the percentage of phagocytic granulocytes was examined by morphology (**B**). Data were analyzed with a Mann–Whitney test using GraphPad Prism 6.0. Bar graphs represent the mean ± SEM of three independent experiments. Asterisks denote significance (****$P < 0.0001$).

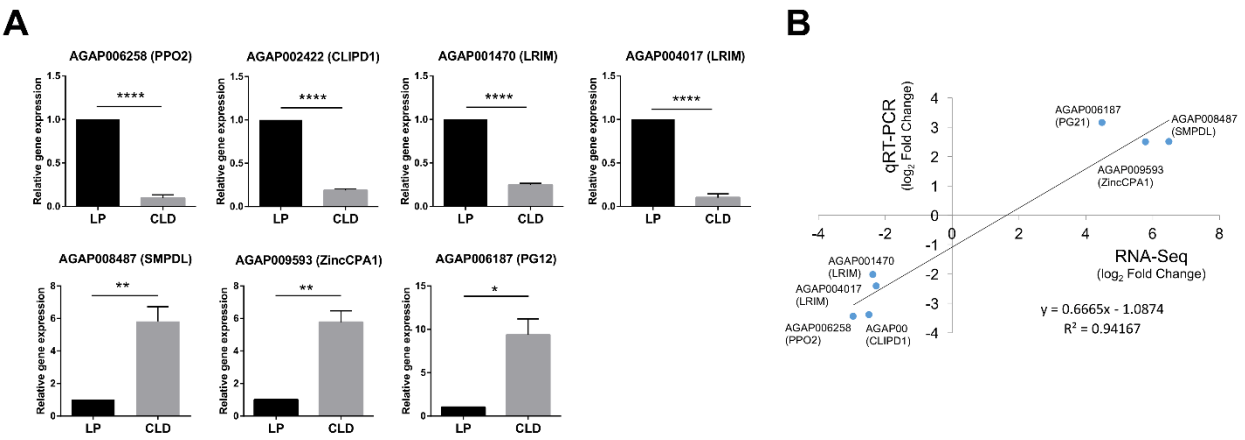

Fig. S10. RNA-seq validation by qRT-PCR. Candidate differentially regulated genes identified in RNA-seq experiments were validated by qRT-PCR using independent control liposome (LP) or clodronate (CLD)-treated mosquito samples (**A**). Relative gene expression is displayed for each gene of interest and represented as the mean ± SEM of three independent experiments. Correlations of gene expression measured between RNA-seq and qRT-PCR data were highly significant (R^2=0.94) (**B**). Gene accession numbers and annotations are displayed above each candidate gene and significance was determined by an unpaired *t*-test using GraphPad Prism 6.0. Asterisks denote significance (*P < 0.05, **P < 0.01, ****P < 0.0001).

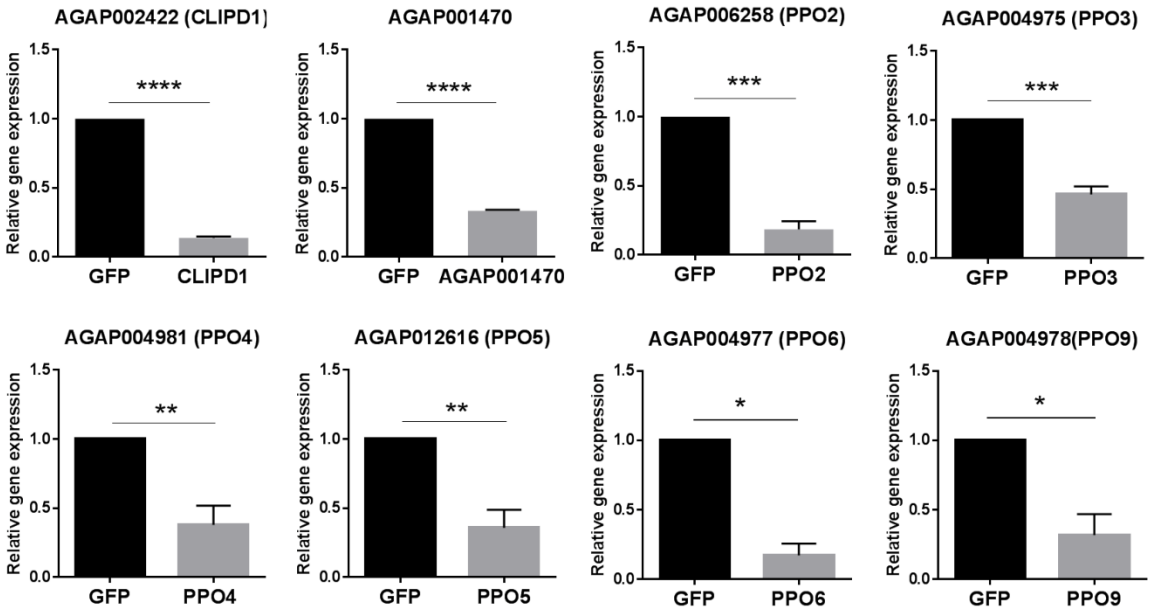

Fig. S11. Validation of dsRNA-mediated gene silencing on candidate immune genes. Gene silencing in candidate immune genes was evaluated by qRT-PCR at day 2 post-injection. Gene expression of the target gene is displayed as the expression level relative to dsGFP-injected control in whole mosquito samples. Gene accession numbers and annotations are displayed above each candidate gene. Data were analyzed by an unpaired *t*-test using GraphPad Prism 6.0. Bar graphs display the mean ± SEM of three independent experiments. Asterisks denote significance (*$P < 0.05$, **$P < 0.01$, ***$P < 0.001$, ****$P < 0.0001$).

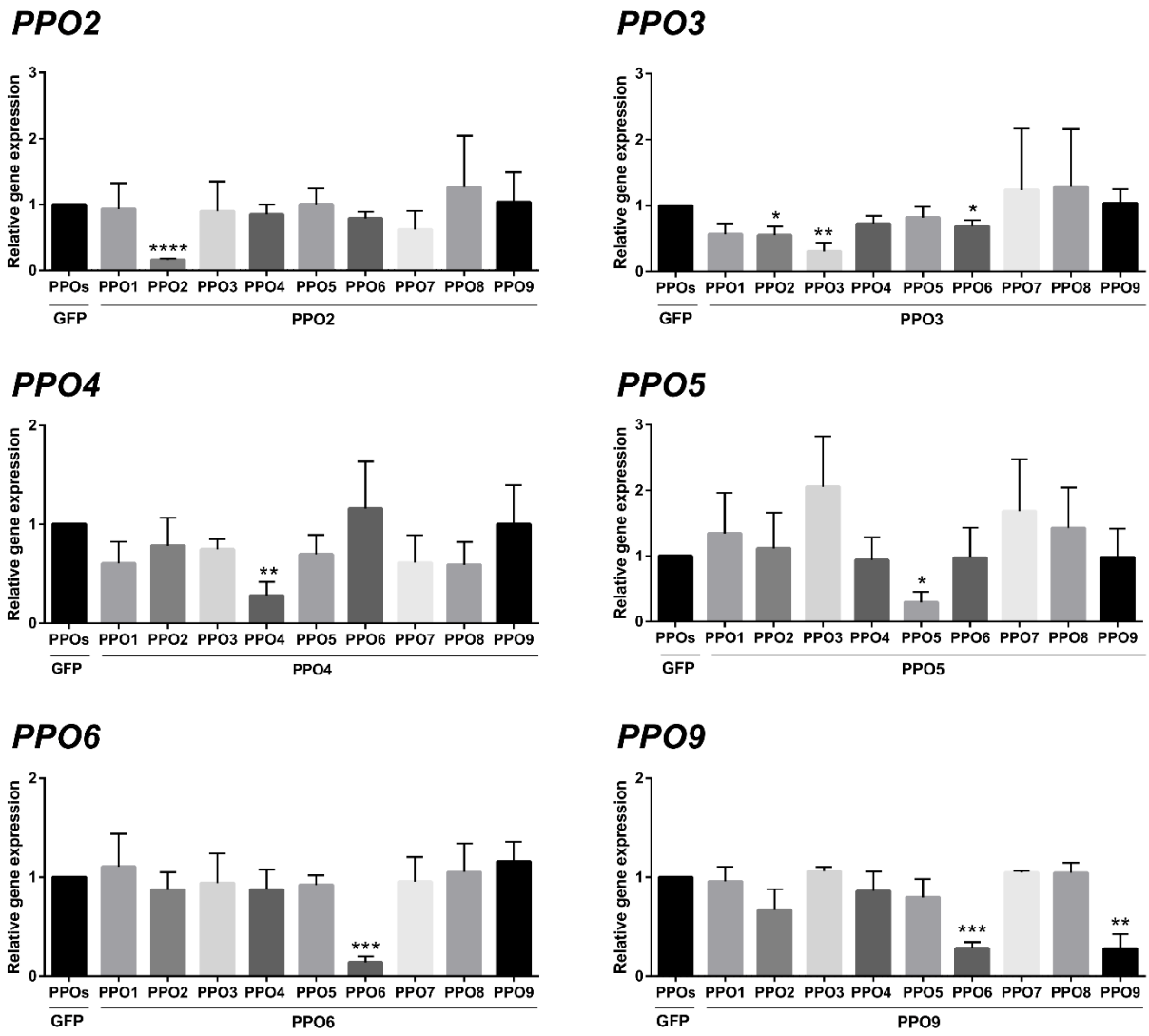

Fig. S12. Analysis of PPO gene family expression following gene-silencing of specific PPO target genes. To determine the specificity of PPO silencing, each dsRNA PPO target was validated across each PPO family to verify if silencing was specific or has potential off-target effect on other multiple PPO transcripts. The relative quantification of all nine PPO transcript levels was analyzed between a specific PPO knockdown and GFP control samples. Data were analyzed by an unpaired *t*-test using GraphPad Prism 6.0. Bar graphs represent mean ± SEM of three independent experiments. Asterisks denote significance (*$P < 0.05$, **$P < 0.01$, ***$P < 0.001$, ****$P < 0.0001$).

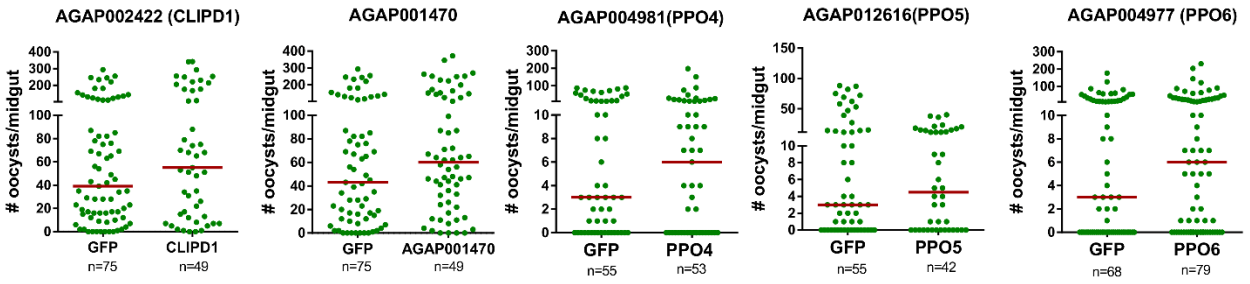

Fig. S13. Evaluation of candidate genes differentially regulated by phagocyte depletion that did not influence malaria parasite survival. Gene-silencing experiments to evaluate *CLIPD1*, *AGAP001470*, *PPO4*, *PPO5*, and *PPO6* did not influence malaria parasite survival. *P. berghei* oocyst numbers were examined at day 8 post-infection. For each candidate gene at least three independent experiments were performed. Data were analyzed by a Mann–Whitney test using GraphPad Prism 6.0. Median is indicated by the horizontal red line.

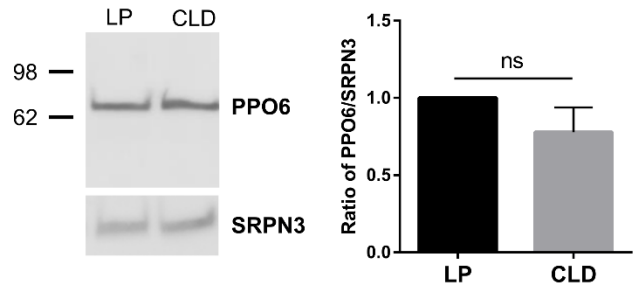

Fig. S14. Evaluation of PPO6 protein levels in mosquito hemolymph. Hemolymph was perfused from control liposome (LP) and clodronate (CLD) treated mosquitoes and evaluated by Western Blot to determine if there were potential differences in PPO6 protein levels. Using SRPN3 as a loading control, no discernable differences were determined between sample treatments by visualization or by quantitation using Image J software.

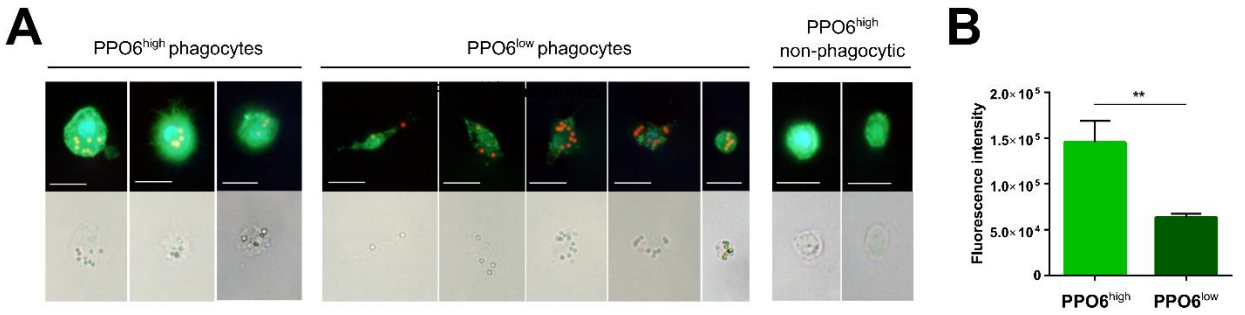

Fig. S15. PPO6 expression and morphology distinguish phagocytic and non-phagocytic immune cell populations in mosquitoes by immunofluorescence. The intensity of PPO6 staining, cell size, and phagocytic ability distinguish immune cell types in perfused hemocytes ~24 h after *P. berghei* infection (**A**). Prior to perfusion, fluorescent beads were injected to determine phagocytic ability to help to distinguish phagocytic cell types (granulocytes) from non-phagocytic cells (oenocytoids and prohemocytes). Immune cell sub-types were detected in both control liposome and clodronate-treated samples. Scale bar: 10 μm. Micrographs of PPO6^{high} and PPO6^{low} cells were evaluated using Image J software to display differences in the fluorescence intensity of these cell types (**B**).

Table S1. Differentially regulated genes as a result of phagocyte depletion

Gene ID	Log2 change	p-value	q-value	Gene name	Gene description	GO Term
AGAP008487	6.501	3.84321E-05	0.013	-	Sphingomyelin phosphodiesterase [Source:UniProtKB/TrEMBL;Acc:Q7Q4M5]	M
AGAP009593	5.761	1.82308E-06	0.001	CP	Zinc carboxypeptidase A 1 [Source:UniProtKB/Swiss-Prot;Acc:O02350]	PROT
AGAP006709	5.539	5.92656E-06	0.002	CHYM1	Chymotrypsin-1 [Source:UniProtKB/Swiss-Prot;Acc:Q27289]	DIG
AGAP007165	5.153	0.000128281	0.034	-	Late trypsin [Source:VB Community Annotation]	PROT
AGAP006187	4.549	0.000194404	0.048	-	Protein G12 [Source:UniProtKB/Swiss-Prot;Acc:Q17040]	D
AGAP006711	4.504	2.11194E-05	0.008	CHYM2	Chymotrypsin-2 [Source:UniProtKB/Swiss-Prot;Acc:Q17025]	DIG
AGAP004860	4.428	0.000412843	0.080	-	protease m1 zinc metalloprotease [Source:VB Community Annotation]	PROT
AGAP005310	4.352	0.00029882	0.067	-	*serine-type enodopeptidase* [Source:UniProtKB/Swiss-Prot]	PROT
AGAP010383	4.254	0.000142676	0.036	-	solute carrier family 15 member 1 [Source:VB Community Annotation]	TRP
AGAP006400	4.124	0.000457303	0.083	-	alkaline phosphatase 2 [Source:VB Community Annotation]	D
AGAP000154	4.069	0.000200742	0.048	-	AMP dependent ligase [Source:VB Community Annotation]	M
AGAP008945	2.791	0.000499908	0.087	ABCG6	ATP-binding cassette transporter (ABC transporter) family G member 6 [Source:VB Community Annotation]	TRP
AGAP010832	2.555	2.74507E-05	0.010	TEP19	thioester-containing protein 19 [Source:VB Community Annotation]	I
AGAP001652	1.555	1.53197E-06	0.001	-	lipase [Source:VB Community Annotation]	M
AGAP009549	1.450	0.000105554	0.029	-	*Placenta growth factor* [Source:UniProtKB/Swiss-Prot]	U
AGAP010479	1.353	5.01503E-05	0.016	-	*Enolase binding protein* [Source:UniProtKB/Swiss-Prot]	D
AGAP028373	1.320	6.48306E-05	0.019	ND3	NADH dehydrogenase subunit 3 [Source:European Nucleotide Archive;Acc:ND3]	M

AGAP002632	1.270	0.000494043	0.087	-	*Putative secreted protein* [Source:UniProtKB/Swiss-Prot]	U
AGAP006001	1.008	0.000444984	0.083	CPR26	cuticular protein RR-1 family 26 [Source:VB Community Annotation]	CS
AGAP009110	0.917	0.000447768	0.083	-	*Putative secreted protein* [Source:UniProtKB/Swiss-Prot]	U
AGAP007349	0.882	9.16299E-05	0.026	-	*Pericardin* [Source:UniProtKB/Swiss-Prot]	D
AGAP009268	-1.024	0.000358655	0.072	-	*vigilin* [Source:UniProtKB/Swiss-Prot]	D
AGAP028064	-1.085	0.000383009	0.076	LRIM16B	leucine-rich immune protein (TM) [Source:VB Community Annotation]	I
AGAP009312	-1.507	1.7466E-09	0.000	-	*SEC14* [Source:UniProtKB/Swiss-Prot]	D
AGAP028028	-1.557	1.66685E-07	0.000	LRIM16A	leucine-rich immune protein (TM) [Source:VB Community Annotation]	I
AGAP004936	-1.569	4.47794E-09	0.000	-	*neurexin iii-alpha* [Source:UniProtKB/Swiss-Prot]	D
AGAP029054	-1.641	3.45071E-07	0.000	NimB2	nimrod B2 [Source:VB Community Annotation]	I
AGAP011197	-1.760	6.48774E-05	0.019	-	*fibrinogen and fibronectin* [Source:UniProtKB/Swiss-Prot]	I
AGAP002134	-1.774	2.44489E-06	0.001	-	*q rich salivary secreted protein* [Source:UniProtKB/Swiss-Prot]	U
AGAP008696	-1.806	1.58547E-05	0.006	-	*Amino acid transporter* [Source:UniProtKB/Swiss-Prot]	TRP
AGAP004016	-1.836	1.82808E-11	0.000	-	*leucine-rich repeat protein* [Source:UniProtKB/Swiss-Prot]	I
AGAP004981	-1.903	5.54882E-07	0.000	PPO4	prophenoloxidase 4 [Source:VB Community Annotation]	I
AGAP012616	-1.929	0.000348639	0.072	PPO5	prophenoloxidase 5 [Source:VB Community Annotation]	I
AGAP001662	-1.950	2.04348E-11	0.000	-	*Papilin* [Source:UniProtKB/Swiss-Prot]	D
AGAP004975	-2.029	0.000318828	0.068	PPO3	prophenoloxidase 3 [Source:VB Community Annotation]	I
AGAP005849	-2.031	5.57925E-05	0.017	-	colmedin [Source:VB Community Annotation]	CS

AGAP006176	-2.053	5.19721E-08	0.000	-	*Laccase-2 isoform B* [Source:UniProtKB/Swiss-Prot]	REDOX
AGAP005340	-2.079	0.000309418	0.067	-	*Putative secreted protein* [Source:UniProtKB/Swiss-Prot]	U
AGAP002422	-2.263	1.30855E-06	0.001	CLIPD1	CLIP-domain serine protease [Source:VB Community Annotation]	I
AGAP001470	-2.362	9.18087E-09	0.000	-	*Leucine-rich repeat-containing protein* [Source:UniProtKB/Swiss-Prot]	I
AGAP010580	-2.378	1.37823E-08	0.000	-	*Mitochondrial genome maintenance exonuclease 1* [Source:UniProtKB/Swiss-Prot]	U
AGAP011228	-2.415	0.000249217	0.059	-	*fibrinogen and fibronectin* [Source:UniProtKB/Swiss-Prot]	I
AGAP000685	-2.478	0.000266195	0.061	-	*Sushi* [Source:UniProtKB/Swiss-Prot]	D
AGAP004017	-2.483	2.58123E-06	0.001	-	*leucine-rich repeat protein* [Source:UniProtKB/Swiss-Prot]	U
AGAP012000	-2.732	1.94498E-06	0.001	-	fibrinogen and fibronectin [Source:VB Community Annotation]	I
AGAP004977	-2.795	3.65512E-07	0.000	PPO6	prophenoloxidase 6 [Source:VB Community Annotation]	I
AGAP004978	-2.870	4.4848E-08	0.000	PPO9	prophenoloxidase 9 [Source:VB Community Annotation]	I
AGAP011223	-2.906	1.07295E-06	0.001	-	*fibrinogen and fibronectin* [Source:UniProtKB/Swiss-Prot]	I
AGAP006258	-2.957	1.87887E-09	0.000	PPO2	prophenoloxidase 2 [Source:VB Community Annotation]	I
AGAP028214	-3.062	3.22838E-10	0.000	-	*histone-lysine N-methyltransferase* [Source:UniProtKB/Swiss-Prot]	U

GO terms: CS, cytoskeletal; D, diverse function; DIG, digestion; I, immunity; M, metabolism; PROT, proteolysis; TRP, transport; U, unknown

Table S2. Primers for qRT-PCR analysis of gene expression

Primer	Sequence (5'-3')	Gene ID
Nimrod B2-qF	CAATCTGCTCAAATGGCTGCTTCCACG	AGAP009762
Nimrod B2-qR	GCTGCAAACATTCGGTCCAGTGCATTC	
eater-qF	TTCACCCGTCTGCGAGGGATGCAAGC	AGAP012386
eater-qR	GTCAACGTGCATAGTAGCGTCTCCGTAGC	
ppo1-qF	GACTCTACCCGGATCGGAAG	AGAP002825
ppo1-qR	ACTACCGTGATCGACTGGAC	
ppo2-qF	TTGCGATGGTGACCGATTTC	AGAP006258
ppo2-qR	CGACGGTCCGGATACTTCTT	
ppo3-qF	CTATTCGCCATGATCTCCAACTACG	AGAP004975
ppo3-qR	ATGACAGTGTTGGTGAAACGGATCT	
ppo4-qF	GCTACATACACGATCCGGACAACTC	AGAP004981
ppo4-qR	CCACATCGTTAAATGCTAGCTCCTG	
ppo5-qF	GTTCTCCTGTCGCTATCCGA	AGAP012616
ppo5-qR	CATTCGTCGCTTGAGCGTAT	
ppo6-qF	GCAGCGGTCACAGATTGATT	AGAP004977
ppo6-qR	GCTCCGGTAGTGTTGTTCAC	
ppo7-qF	CAGCGATTGACGAAGGTGTT	AGAP004980
ppo7-qR	GAAAGCAATACGTGCCCACT	
ppo8-qF	CCTTTGGTAACGTGGAGCAG	AGAP004976
ppo8-qR	CTTCAAACCGCGAGACCATT	
ppo9-qF	TGTATCCATCTCGGACGCAA	AGAP004978
ppo9-qR	AAGGTTGCCAACACGTTACC	
clipd1-qF	CAAGCAGTTCAACGAAACGC	AGAP002422
clipd1-qR	AAGGACGGCTGTATCAGCTT	
lrim-qF	GAAGGTAAGCTCCGACACCT	AGAP001470
lrim-qR	CTGGCCGGCCTGCTCGAGCT	
lrim-qF	TGTGAACGGGCTAAAGGAGT	AGAP004017
lrim-qR	AAAGAGTCGCAGCTTTGGTG	
smpdl-qF	CGCTACTGGGAGTACAAGGT	AGAP012386
smpdl -qR	TCCGACAGCTCTTGACACTT	
zinccp-qF	CGGTAAAGTCACTGGCGAAG	AGAP009593
zinccp-qR	GCTCGTACGTGTACGCAATC	
Pg12-qF	CCTGACCGACGATTTCGATG	AGAP006187
pg12-qR	GAGTCTGCTGCACCTCCTTA	
rps7-qF	ACCACCATCGAACACAAAGTTGACACT	AGAP010592
rps7-qR	CTCCGATCTTTCACATTCCAGTAGCAC	

Table S3. Primers for the production of dsRNA used in gene-silencing experiments

Primer	Sequence (5'-3')	Gene ID
ppo2-T7F	TAATACGACTCACTATAGGGTTTGAGTTCTGCCTCAGCAA	AGAP006258
ppo2-T7R	TAATACGACTCACTATAGGGATGCTTCGGCGCAAATAG	
ppo3-T7F	TAATACGACTCACTATAGGGGCACCATCTGCTAATTCCGA	AGAP004975
ppo3-T7R	TAATACGACTCACTATAGGGTGTGTCAGTAATCGTTTGCCA	
ppo4-T7F	TAATACGACTCACTATAGGGATCCCCGAGGCGTACTTTC	AGAP004981
ppo4-T7R	TAATACGACTCACTATAGGGCGTTGTTGTGAAGATCTCCGT	
ppo5-T7F	TAATACGACTCACTATAGGGGCGTACCTAACGGACCAGTA	AGAP012616
ppo5-T7R	TAATACGACTCACTATAGGGACAGTTCCAGAAAGCTCGGT	
ppo6-T7F	TAATACGACTCACTATAGGGAGCTGTATCCCGATAAGCGTC	AGAP004977
ppo6-T7R	TAATACGACTCACTATAGGGGCCTCGATCGCAGAATTAAC	
ppo9-T7F	TAATACGACTCACTATAGGGCGGGCAGTGCATCAAGTT	AGAP004978
ppo9-T7R	TAATACGACTCACTATAGGGTAGATTAAATTCACCGTGGCG	
clipd1-T7F	TAATACGACTCACTATAGGGCGTTAGTTCGGTGTCGTGAA	AGAP002422
clipd1-T7R	TAATACGACTCACTATAGGGCGTGTGCGACATTCCTTG	
lrim-T7F	TAATACGACTCACTATAGGGAACCACCAACCGTACTGGAC	AGAP001470
lrim-T7R	TAATACGACTCACTATAGGGCCGTAGAACGCAAACGGT	
GFP-T7F	TTAATACGACTCACTATAGGGAGAATGGTGAGCAAGGGCGAGGAGCTGT	
GFP-T7R	TTAATACGACTCACTATAGGGAGATTACTTGTACAGCTCGTCCATGCC	

References

1. Andrews S (2010) FastQC: a quality control tool for high throughput sequence data. Available at: http://www.bioinformatics.babraham.ac.uk/projects/fastqc.

2. Giraldo-Calderón GI, et al. (2015) VectorBase: An updated bioinformatics resource for invertebrate vectors and other organisms related with human diseases. *Nucleic Acids Res* 43(D1):D707–D713.

3. Dobin A, et al. (2013) STAR: Ultrafast universal RNA-seq aligner. *Bioinformatics* 29(1):15–21.

4. Li H, et al. (2009) The sequence alignment/map format and SAMtools. *Bioinformatics* 25(16):2078–2079.

5. Liao Y, Smyth GK, Shi W (2014) FeatureCounts: An efficient general purpose program for assigning sequence reads to genomic features. *Bioinformatics* 30(7):923–930.

6. Robinson MD, McCarthy DJ, Smyth GK (2009) edgeR: A Bioconductor package for differential expression analysis of digital gene expression data. *Bioinformatics* 26(1):139–140.

7. Edgar R, Domrachev M, Lash AE (2002) Gene Expression Omnibus: NCBI gene expression and hybridization array data repository. *Nucleic Acids Res* 30(1):207–210.

8. Horn T, Boutros M (2010) E-RNAi: A web application for the multi-species design of RNAi reagents-2010 update. *Nucleic Acids Res* 38(SUPPL. 2):332–339.

9. Smith RC, et al. (2016) Molecular profiling of phagocytic immune cells in *Anopheles gambiae* reveals integral roles for hemocytes in mosquito innate immunity. *Mol Cell proteomics* 15(11):3373–3387.

10. Povelones M, et al. (2013) The CLIP-domain serine protease homolog SPCLIP1 regulates complement recruitment to microbial surfaces in the malaria mosquito *Anopheles gambiae*. *PLoS Pathog* 9(9):e1003623.

11. Michel K, et al. (2006) Increased melanizing activity in *Anopheles gambiae* does not affect development of *Plasmodium falciparum*. *Proc Natl Acad Sci U S A* 103:16858–16863.

12. Rodrigues J, Brayner FA, Alves LC, Dixit R, Barillas-Mury C (2010) Hemocyte differentiation mediates innate immune memory in *Anopheles gambiae* mosquitoes. *Science* 329:1353–1355.

13. Garver LS, de Almeida Oliveira G, Barillas-Mury C (2013) The JNK pathway is a key mediator of Anopheles gambiae antiplasmodial immunity. *PLoS Pathog* 9(9): e1003622.

14. Ramirez JL, et al. (2014) The role of hemocytes in *Anopheles gambiae* antiplasmodial immunity. *J Innate Immun* 6:119–128.

15. Smith RC, Barillas-Mury C, Jacobs-Lorena M (2015) Hemocyte differentiation mediates the mosquito late-phase immune response against *Plasmodium* in *Anopheles gambiae*. *Proc Natl Acad Sci* 112:E3412-20.

16. Ramirez JL, et al. (2015) A mosquito lipoxin/lipocalin complex mediates innate immune priming in *Anopheles gambiae*. *Nat Commun* 6:7403.

17. Kwon H, Arends BR, Smith RC (2017) Late-phase immune responses limiting oocyst survival are independent of TEP1 function yet display strain specific differences in *Anopheles gambiae*. *Parasit Vectors* 10(1):369.

18. Castillo JC, Robertson AE, Strand MR (2006) Characterization of hemocytes from the mosquitoes Anopheles gambiae and Aedes aegypti. *Insect Biochem Mol Biol* 36:891–903.

19. Baton LA, Robertson A, Warr E, Strand MR, Dimopoulos G (2009) Genome-wide transcriptomic profiling of *Anopheles gambiae* hemocytes reveals pathogen-specific signatures upon bacterial challenge and *Plasmodium berghei* infection. *BMC Genomics* 10:257.

20. Castillo J, Brown MR, Strand MR (2011) Blood feeding and insulin-like peptide 3 stimulate proliferation of hemocytes in the mosquito *Aedes aegypti*. *PLoS Pathog* 7(10):e1002274.

21. Oliver JD, Dusty Loy J, Parikh G, Bartholomay L (2011) Comparative analysis of hemocyte phagocytosis between six species of arthropods as measured by flow cytometry. *J Invertebr Pathol* 108(2):126–130.